Nitrogen Doped $Sr_2Ta_2O_7$ Coupled with Graphene Sheets as Photocatalysts for Increased Photocatalytic Hydrogen Production

Aniruddh Mukherji, Brian Seger, Gao Qing (Max) Lu,* and Lianzhou Wang*

ARC Centre of Excellence for Functional Nanomaterials, School of Chemical Engineering and Australian Institute for Bioengineering and Nanotechnology, The University of Queensland, St Lucia, Brisbane, QLD 4072 Australia

ABSTRACT In this work we present the synthesis of a new type of nitrogen-doped tantalate, $Sr_2Ta_2O_{7-x}N_x$, which exhibited significantly increased visible light absorption and improved photocatalytic hydrogen production by 87% under solar irradiation, compared with its undoped counterpart $Sr_2Ta_2O_7$. The photocatalyst also exhibited a strong capability in photoinduced reduction of exfoliated graphene oxide (GO) to graphene sheets. By using graphene as a support for a Pt cocatalyst, a new type of composite containing graphene-Pt and $Sr_2Ta_2O_{7-x}N_x$ was designed, which demonstrated an additional ~80% increase in hydrogen production and an quantum efficiency of 6.45% (~177% increase from pristine undoped $Sr_2Ta_2O_7$) due to the efficient charge carrier separation on the photocatalyst. This work suggests that graphene can play an important role as an electron transfer highway, which facilitates the charge carrier collection onto Pt cocatalysts. The method can thus be considered as an excellent strategy to increase photocatalytic hydrogen production in addition to a commonly applied doping method.

KEYWORDS: photocatalysts · graphene · hydrogen production · visible light photoactivity · electron transfer

Hydrogen as a clean and renewable energy carrier has attracted much recent R&D attention.[1−4] Among the many reported methods for H_2 generation outside of the carbon cycle, the solar-driven water splitting process in the presence of a semiconductor photocatalyst has been considered as one of the ultimate routes.[5,6] The properties responsible for photocatalytic water splitting have been identified and well documented over the years. However it has been a challenge to date to find materials that satisfy all the necessary requirements. Among a variety of hydrogen production photocatalysts, tantalum oxide based compounds have been reported to be very active.[7−9] The conduction band (CB) of these tantalate based photocatalysts consists of Ta 5d orbitals and the valence band (VB) consists of O2p orbitals. It is known that Ta^{5+} has excess overpotentials for reduction of H^+ to H_2, which is higher than most other d^0 elements. It has also been suggested that the closer the O−Ta−O bond is to 180°, the more the excitation energy is delocalized,[9,10] indicating that electron−hole pairs generated as a result of photoexcitation can be mobilized easily in photocatalysts containing TaO_6 octahedra. This suggests that layered perovskite-type materials containing TaO_6 octahedra are suitable candidates for water splitting. For instance, $Sr_2Ta_2O_7$, as a wide band gap layered perovskite-type semiconductor, has been reported to be an active water splitting photocatalyst in the ultraviolet (UV) region.[11]

However, most of existing photocatalyst materials like the above-mentioned $Sr_2Ta_2O_7$ and well-known TiO_2 are mainly active under UV light irradiation because of their wide band gap (usually 3.0−4 eV).[7,8,10] Considering the percentage of UV light is less than 5% of the total solar spectrum incident on the earth, in the past decade it has been a research focus to explore photocatalyst materials which can efficiently utilize visible light. An appropriate photocatalyst should function in the visible light region (420 nm < λ < 800 nm) with a band gap of less than 3 eV. Thus band gap engineering of photocatalysts to induce absorption into the wide visible light region has been considered as a possible solution to this problem. The doping of anions such as N,[12,13] S,[14,15] P,[16] and C[16] into known wide band gap semiconductors, mainly TiO_2, has been reported. This approach was pioneered by Asahi *et al.*[12] Ever since then nitrogen doping has emerged as a generic way of reducing the band gap of semiconductor photocatalysts. Domen and his co-workers group have made significant progress in recent years by developing TaON and many other tantalum oxy-nitrides

* Address correspondence to l.wang@uq.edu.au, maxlu@uq.edu.au.

Received for review September 20, 2010 and accepted April 13, 2011.

Published online April 13, 2011
10.1021/nn102469e

including perovskite oxy-nitrides.[9,17−19] It is now generally recognized that efficiency of anion doping can be related to structural shortcomings of most photocatalysts. Nonhomogenous doping combined with long diffusion lengths within the bulk of the photocatalysts before reaching surface active sites could play a crucial role in determining the efficiency. We recently reported a new strategy to realize homogeneous nitrogen doping which exhibited significantly improved visible light absorption and better photocatalytic properties. The layered perovskite structure was crucial in achieving homogeneous doping.[20] A similar strategy was also employed to a tunnelled pyrochlore structure, and the material showed a remarkable 2-fold increase in photocatalytic hydrogen generation performance.[21] This idea forms a good basis for achieving further improved visible light activity by nitrogen doping UV-active other layered compounds like perovskite-type $Sr_2Ta_2O_7$, while a number of additional factors still need to be considered and optimized in order to design new photocatalysts with higher photocatalytic performance.

The quantum efficiency, one of the most appropriate measures in evaluating the performance of photocatalysts, depends highly on ratio between charge carrier transfer rate and the electron−hole recombination rate. Time resolved spectroscopic studies have confirmed that approximately 90% of electron−hole pairs recombine rapidly after excitation,[22,23] which is no doubt a serious issue to be addressed in the field. Improving the quantum efficiency would necessarily involve understanding and controlling the interaction between the electronic, crystallographic and surface properties by a systematic and rational approach toward designing active and efficient photocatalysts. There has been much effort to date to improve efficiencies by using cocatalysts like Pt, Rh, NiO, and RuO_2,[8,10,19,20,24] which can affect the overall recombination rate, but the extent of success has been limited. The interaction between the semiconductors and the cocatalysts in heterogeneous material systems remains complicated, and more investigation is warranted.

The use of carbon scaffolds to improve dispersion and surface area of electrocatalysts was one of the major breakthroughs in the field of fuel cell technologies.[25] More recently carbon supports have been used as a scaffold to increase photocurrent for solar cell applications with impressive success.[26,27] However the use of carbon scaffolds and its effect on increased efficiencies has not been widely reported. Among carbon based materials, layered graphite and graphene oxide has shown excellent physical properties; however, the isolation and separation of single layers have been a challenge. Ever since the single carbon sheet, graphene, was first isolated in 2004,[28] the material has offered exciting new opportunities in various different fields of nanotechnology. Due to graphene's two-dimensional structure with sp^2-bonded carbon atoms arranged in a honeycomb structure, its applications have been explored particularly in the fields of electronic and catalytic fields. It has been previously reported that graphene offers excellent charge mobility (200 000 $cm^2\ V^{-1}\ s^{-1}$), high theoretical surface area (2620 m^2/g) and high transparency.[29−31] Because of graphene's large network of sp^2 hybridized carbon, this material tends to form strong $\pi-\pi$ bonds with other graphene sheets to form graphite. One of the most common methods to separate the sheets is to oxidize the carbon by attaching functional groups such as alcohols, epoxide, and carboxylate groups forming graphene oxide (GO).[32,33] This both delaminates the graphite into single graphene sheets and adds polar groups to allow the material to be soluble in polar solutions. A pitfall of this method is that the oxidation destroys the sp^2 hybridized network and thus the conductivity of the material. However, GO can be converted to the much more conductive graphene by chemical reduction with materials such as hydrazine or HI.[34] Recently Williams *et al.*[35,36] successfully demonstrated that it was possible to photocatalytically reduce GO using UV active photocatalysts. Using such oxidation and reduction techniques, researchers have been able to effectively use the graphene in a broader range of fields from solar cells,[37] to fuel cells,[38] to batteries.[39] During the writing of this manuscript Ng *et al.*[40] showed great enhancement with graphene oxide as a scaffold for photoelectrochemical water oxidation and photocurrent generation on a semiconductor $BiVO_4$ thin film. Because of the effective results in fuel cells and photocurrent generation, there appears to be great untapped potential of using carbon nanostructures to help improve hydrogen production.

In light of the above-mentioned points, the key issues which limit the efficiency of a photocatalyst include (1) the inability of photocatalyst to utilize visible light (>420 nm) and (2) high rate of recombination of charge carriers in such photocatalyst. In this work we look at using two strategies in synchronization to improve the photocatalytic hydrogen production. In the first endeavor we took the UV active layered $Sr_2Ta_2O_7$, and doped it with nitrogen to minimize the band gap thus allowing visible light absorption. In the presence of a standard platinum cocatalyst, we demonstrated that the doped catalyst resulted in nearly double hydrogen yield than the undoped counterpart. The second strategy we used to further improve photocatalytic hydrogen production was to use graphene, which was acquired by using $Sr_2Ta_2O_{7-x}N_x$ to reduce GO under visible light irradiation, as a scaffold, or charge carrier transport "highway," to shuttle electrons to the platinum cocatalysts. This strategy was expected to significantly mitigate the recombinatory reactions of charge carriers, thus facilitating the electron transfer to photocatalysts surfaces for hydrogen production reaction, as schematically illustrated in

Figure 1. Using both doped $Sr_2Ta_2O_7$ and the reduced GO as scaffolds with Pt decorated on them, we were able to increase photocatalytic hydrogen production substantially.

RESULTS AND DISCUSSION

Nitrogen Doping of $Sr_2Ta_2O_7$ for Increased Visible Light Absorption. $Sr_2Ta_2O_7$ was synthesized using a reported procedure by a solid state reaction method.[12] The perovskite material was then doped in an ammonia atmosphere as discussed in the Experimental Section. Figure 2 shows the UV–vis absorption spectra for $Sr_2Ta_2O_7$ and nitrogen doped $Sr_2Ta_2O_{7-x}N_x$. The N doping resulted in the shifting of the absorption edge from 290 nm to nearly 550 nm in the visible light region. The band gap was estimated from the Kubelka–Munk function *versus* the energy of the light absorbed to be *ca.* 2.3 eV (details in Supporting Information), which is significantly lower compared to that of $Sr_2Ta_2O_7$ (4.2 eV). The shift in the absorption spectra was also indicated by the change in color of the powders from white to bright yellow. Utilizing visible light for driving photocatalytic reactions is a key challenge since most oxides only absorb UV light. In contrast to the pristine $Sr_2Ta_2O_7$, $Sr_2Ta_2O_{7-x}N_x$ exhibited a large red shift in absorbance. This shift in the absorbance is quite different and far pronounced than the commonly observed absorption shoulders. The steep absorption edges of the $Sr_2Ta_2O_{7-x}N_x$ and the almost parallel characteristics of the absorption edges are significant due to the large shift in band gap. As discussed in our previous report,[11] the layered structure can offer diffusion pathways allowing for much easier nitrogen penetration into the crystal lattice resulting in a more uniform doping. This uniform doping helps promote the total red shift of the absorption, being different from the commonly observed shoulder absorption. We recently reported the successful nitrogen doping of a new tantalum tungstate material which showed a similar effect after nitrogen doping.[21] The results depicted suggest that uniform nitrogen doping carried out by the relatively simple process of annealing had induced visible light absorption in the material. Elemental analysis was carried out using a flash elemental analyzer. It was determined that 0.905 wt % nitrogen was doped into $Sr_2Ta_2O_7$.

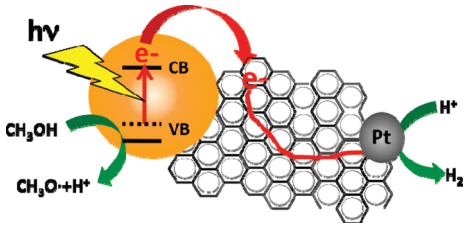

Figure 1. Schematic diagram for charge carrier separation and photocatalytic H_2 production on Pt-loaded graphene-$Sr_2Ta_2O_{7-x}N_x$ photocatalyst under simulated solar light irradiation.

Figure 3 shows the XRD patterns of pristine $Sr_2Ta_2O_7$ and $Sr_2Ta_2O_{7-x}N_x$. It is evident that there is nearly no change in the crystal structure of $Sr_2Ta_2O_7$ after N-doping. It was suggested by Ji *et al.*[41] that the extent of nitrogen doping is very important for optimizing photocatalytic performance of the photocatalysts. Nitridation beyond an extent to which alters the crystal lattice has proven to be detrimental to photocatalysis performance. Thus, retaining the original crystal structure of the photocatalyst is vital to their functionality. From Figure 3 it was clear that nitrogen doping had a negligible effect on the crystal structure of our material.

To investigate the state of the nitrogen dopant in $Sr_2Ta_2O_{7-x}N_x$, N1s core levels were measured using XPS. The results have been depicted in Figure 4. A strong

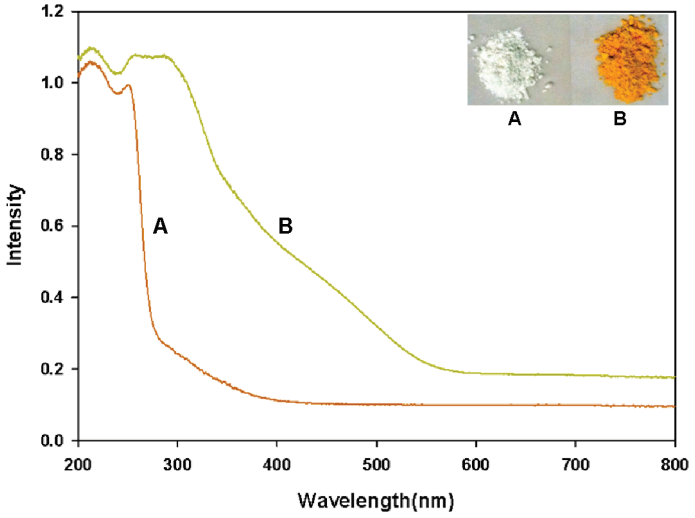

Figure 2. UV–visible spectra of (A) $Sr_2Ta_2O_7$ and (B) $Sr_2Ta_2O_{7-x}N_x$; inset shows the color change from white (A) to bright yellow (B) upon N-doping.

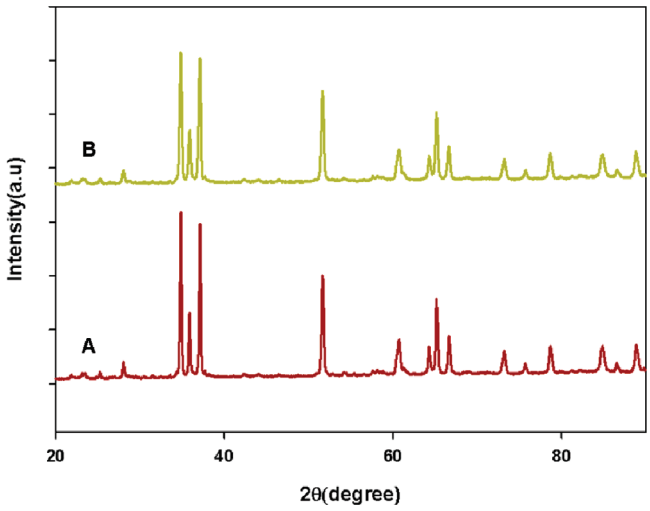

Figure 3. XRD patterns of (A)$Sr_2Ta_2O_7$ and (B) $Sr_2Ta_2O_{7-x}N_x$.

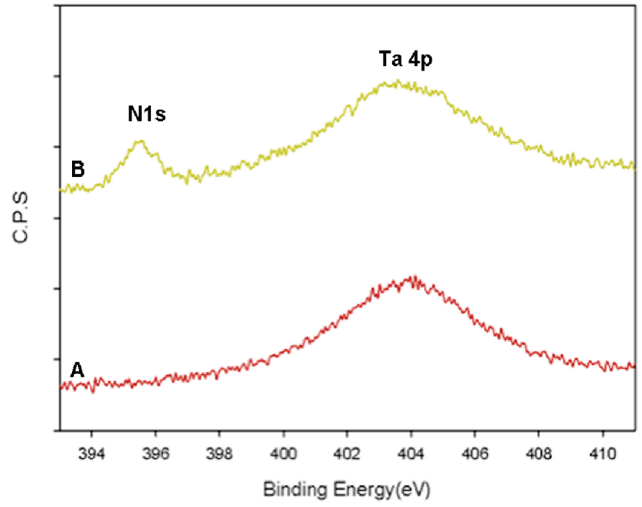

Figure 4. XPS spectra of (A) $Sr_2Ta_2O_7$ and (B) $Sr_2Ta_2O_{7-x}N_x$.

peak at *ca.* 404 eV was evident in all the XPS scans. This can be attributed to the Ta $4p(^3/_2)$, due to the abundance of Ta in both the samples. After nitrogen doping a new peak centered at 395.2 eV appeared for $Sr_2Ta_2O_7$ in addition to the peak at 404 eV. A number of studies have recently confirmed that doped nitrogen with binding energy at around 395 eV can be attributed to β-N.[11,13,14,42] This suggests that within the bilayers consisting of Ta−O bonds small portions of Ta−N bonds were formed by the doped nitrogen. This might be reasonably explained because the N/N−H/N−H_2 species, derived from the decomposition of NH_3 molecules, can migrate into the interlayer galleries of the perovskite structure, which readily replaces the oxygen in $Sr_2Ta_2O_7$ to realize homogeneous nitrogen doping in the material.

The H_2 production efficiency of pristine $Sr_2Ta_2O_7$ and $Sr_2Ta_2O_{7-x}N_x$, each with 0.5 wt % Pt loaded, was measured under simulated solar light irradiation (AM1.5, 1000 W/m^2). AM1.5 contains only a small amount of UV light (<5%), thus this test will allow us to analyze the predominately visible photocatalytic capabilities of these photocatalysts. The photocatalysts were stirred in an aqueous suspension with methanol as a sacrificial agent (electron donor). Platinum has been reported to be a cocatalyst for H_2 production and it has been shown that 0.5 wt % was the optimum concentration. As shown in Figure 5 excellent photocatalytic activity was confirmed for $Sr_2Ta_2O_{7-x}N_x$ and was considerably higher compared to the undoped counterpart. The maximum H_2 production rate achieved for the nitrogen doped material was 194 μM/hour (±5%) compared to 106 μM/hour (±5%) for the undoped material. The evolved gases were sampled continuously using an online quadropole mass spectrometer and the photocatalyst exhibited very high stability under the same experimental conditions over a course of 30 h.

The positions of the valence band maximum (VBM) and the conduction band minimum (CBM) are critical

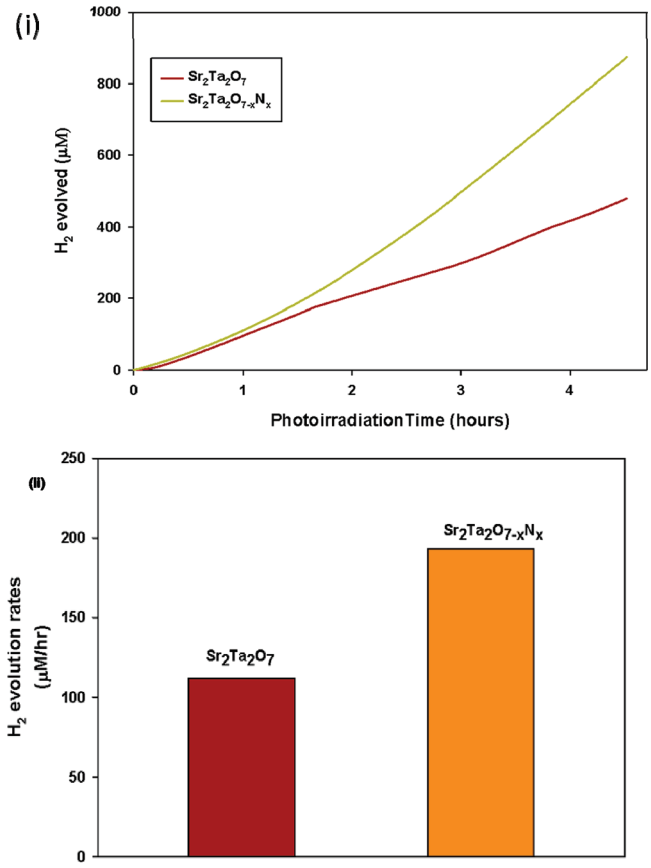

Figure 5. Hydrogen evolution rates of $Sr_2Ta_2O_7$ and $Sr_2Ta_2O_{7-x}N_x$ using Pt as the cocatalyst: (i) total hydrogen produced in a course of 4.5 h; (ii) hydrogen evolution rates per hour.

variables in determining the feasibility of solar hydrogen production. A photocatalyst exhibiting spontaneous water splitting must have a band gap of greater than 1.23 V, with the CBM higher than the H^+/H reduction potential. However due to the large overpotential typically found in the water oxidation reaction, the band gap should be significantly larger. As exemplified in some of our earlier works[11,21] involving Density Functional Theory (DFT) and first principal calculations, the increase in the VBM without altering the CBM as a result of N-doping reduces the overall band gap and thus forms intermediate steps higher than the VBM formed as a result of N2p and O2p orbital mixing. This leads to much greater visible light absorption, which may eventually result in increased H_2 production yields as demonstrated. The increase in hydrogen production activity after nitrogen doping was almost doubled. The quantum efficiency of the doped system was calculated to be 4.26%, which was considerably higher compared to the value of 2.33% for the undoped system. Both efficiencies were calculated in the wavelength region of 280 to 550 nm for an AM1.5 light source (details in Supporting Information). This implied that the nitrogen doping leads to more photons being absorbed by the photocatalyst, which subsequently results in an increase in generating charge carriers and an improvement of quantum efficiency.

Photoinduced Reduction of Graphene Oxide (GO) in the Presence of $Sr_2Ta_2O_{7-x}N_x$. GO-$Sr_2Ta_2O_{7-x}N_x$ composite photocatlaysts were prepared by first using an ultrasonic probe to sonicate and exfoliate GO particles in methanol. Subsequently the as-prepared $Sr_2Ta_2O_{7-x}N_x$ was added and sonicated with the suspended GO single sheets in methanol to ensure good mixing of the materials.

A UV–vis spectrum of the composite in methanol solution was taken initially. The material was then stirred and irradiated with AM1.5 solar irradiation, and subsequently the samples were analyzed at regular time intervals of every 60 min. The UV–visible spectrum for the GO-$Sr_2Ta_2O_{7-x}N_x$ composite in 100% methanol is shown in Figure 6. A very steady change in the absorption spectrum of the GO-$Sr_2Ta_2O_{7-x}N_x$ (1:1 by weight) suspension was recorded. The change in absorption in the visible light region (400–700 nm) was also evident by the color change of the suspension as shown in the inset of Figure 6. This color change from canary yellow to brown/black is due to the partial restoration of π bonds within the carbon structure.[43,44] In the absence of photocatalyst there was no change in the UV–vis spectrum after solar irradiation. It should be noted that the GO suspends well in aqueous solution while the photocatalyst does not. Even though a stirrer was used to mix the material, there was still not always

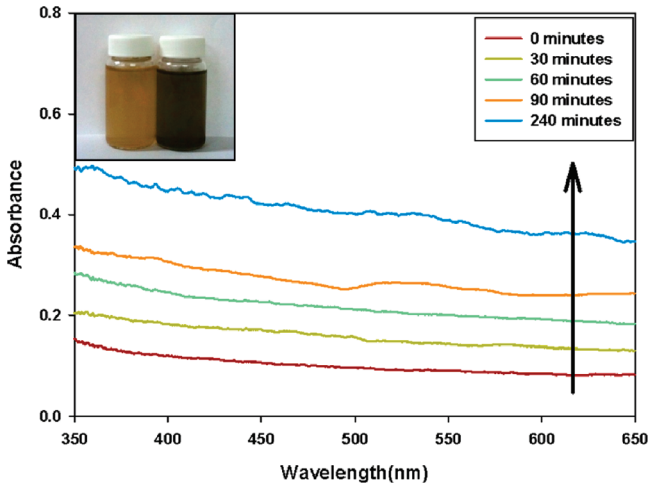

Figure 6. The absorption spectra of GO and $Sr_2Ta_2O_{7-x}N_x$ suspensions under simulated solar irradiation from 0 to 300 min (indicated by the arrow). The inset shows the color change of methanol solution from yellow to black (10 mL containing 0.5 mg/mL of $Sr_2Ta_2O_{7-x}N_x$ and 0.5 mg/mL of GO).

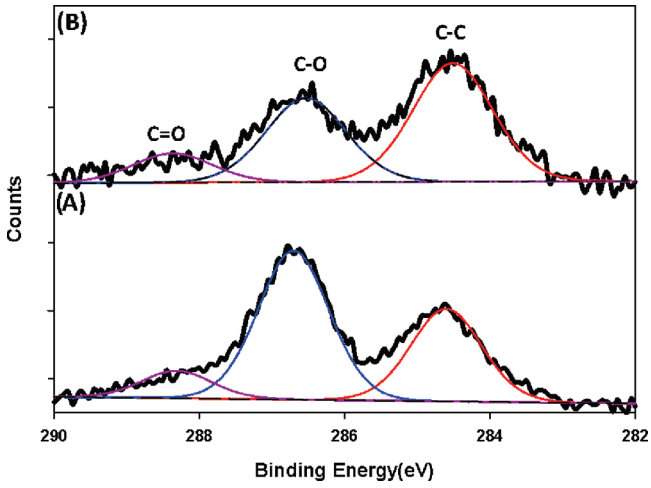

Figure 7. XPS C1s spectra of $Sr_2Ta_2O_{7-x}N_x$-GO composite (1:1 by mass): (A) before and (B) after photocatalytic reduction.

intimate contact between photocatalyst and graphene. This may be a factor in the long time it took to photoreduce the material compared to other dispersible photocatalysts.[35,36]

The photoinduced reduction of graphene oxide was analyzed using X-ray photoelectron spectroscopy (XPS). C1s spectra of $Sr_2Ta_2O_{7-x}N_x$-GO composites (1:1 by mass) before and after being irradiated with simulated solar irradiation are as shown in Figure 7. The peak centered at 284.5 eV is attributed to nonoxygenated C−C linkages while the C−O linkage is centered at *ca.* 286.6 eV. There was an appreciable drop in the peak intensity (counts) after irradiation in the presence of the photocatalyst. This clearly illustrates that photocatalytic deoxygenation was effectively carried out during the course of irradiation. These results were further verified by Fourier transform infrared (FTIR) spectroscopic studies as shown in the Supporting Information, Figure S4. It was evidenced that the photoirradiated sample had lesser stretching at 1060 cm^{-1} (C−O stretching vibrations) and 1600 cm^{-1} (C−O stretching vibrations). The stretching vibrations in the range of 800−400 cm^{-1} could be attributed to the Ta−O linkages in the photocatalyst $Sr_2Ta_2O_{7-x}N_x$. XRD patterns (Supporting Information, Figure S5) for the $Sr_2Ta_2O_{7-x}N_x$-GO composites (1:1 by mass) before and after photoirradiation were also examined. The sample before irradiation did show a XRD peak at ∼15.2° which may be attributed to the (001) plane of GO, but this peak was not observed after the photoirradiation of the sample. Ng *et al.*[40] suggested that this loss of the peak may be attributed to the loss of oxygen functional groups, which leads to structural changes and the disappearance of the (001) peak after photoirradiation. When light strikes the photocatalyst the promoted electron in the CB is at a high enough reduction potential to reduce some of the functional groups on the GO. The methanol acts to scavenge the hole from the photocatalyst. While UV active photocatalysts such as TiO_2, and ZnO have shown to

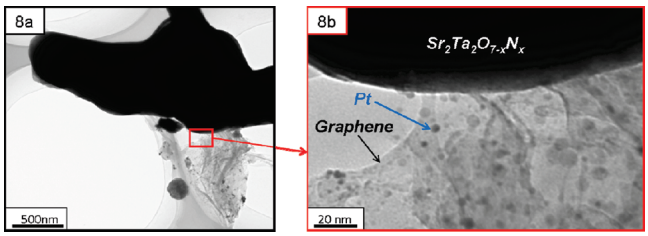

Figure 8. TEM images (a and b) of Graphene-$Sr_2Ta_2O_{7-x}N_x$, showing that the $Sr_2Ta_2O_{7-x}N_x$ particle is in contact with graphene sheets and the Pt particles are deposited uniformly on the graphene sheets.

photoreduce GO.[35,36] In this work, we used a visible light photocatalyst to reduce GO. Because of the higher CB level of $Sr_2Ta_2O_{7-x}N_x$ than that of TiO_2 or ZnO,[6,30] the tantalum oxide species also has the potential to inject higher energy electrons into the GO to reduce more functional groups. Note that some stretching vibrations are still observable in the FTIR spectra, thus this method does not appear to completely reduce GO to graphene. However, maintaining some functionalization allows the GO to still be easily suspended in aqueous solution.

Water Splitting for Hydrogen Production Using Graphene-$Sr_2Ta_2O_{7-x}N_x$ Composites. The above-reported procedure was slightly modified for carrying out photocatalytic efficiency measurements with graphene-$Sr_2Ta_2O_{7-x}N_x$. Noble metal loading is a well-established method for increasing H_2 yield in water splitting, and Pt loading is known to have a significant impact on H_2 production yields. In our study, platinum was loaded onto GO particles using an earlier reported procedure. This was mixed with the photocatalyst so that the GO-Pt was 5 wt % of the total solution. Thus the $Sr_2Ta_2O_{7-x}N_x$ to Pt ratio was 0.5 wt %, which is typically the standard Pt concentration for most photocatalytic hydrogen production systems.[7−9] Figure 8a shows that both a few isolated $Sr_2Ta_2O_{7-x}N_x$ particles and a large agglomeration were attached to the graphene sheets, indicating that the graphene sheets have very good interaction with the photocatalyst particles. Figure 8b visualizes that the Pt nanoparticles are well dispersed on the graphene sheet with a size of 4−10 nm. High resolution TEM images indicate the crystallinity and distribution of Pt nanoparticles and $Sr_2Ta_2O_{7-x}N_x$ material (Supporting Information Figures S2 and S3).

Figure 8b also shows that there is minimal direct contact between the photocatalyst and the platinum in this composite, thus the electron must travel through the graphene to the platinum particle if the support is to be effective. The photocatalytic reduction of the GO earlier in this work has already shown that electrons can be inserted to the GO to reduce the functional groups, but photocatalytic hydrogen production tests were needed to determine the effectiveness of electron transfer to and through graphene to the Pt cocatalyst.

Photocatalytic Hydrogen Production. Different amounts of graphene (2.5−10 wt %) were mixed with $Sr_2Ta_2O_{7-x}N_x$ to test for photocatalytic hydrogen evolution efficiency using methanol as a scavenger. The solution in the photocatalytic reactor was purged with argon for 3 h under dark conditions. The composite was then photoirradiated to carry out photoreduction of the graphene oxide and photocatalytic hydrogen measurements.

It should be noted that when the platinum metal was reduced onto GO *via* sodium borohydride, the sodium borohydride could also partially reduce the support GO,[37] providing some degree of conductivity. This allows electrons to pass from the photocatalyst through the graphene to the platinum for hydrogen production. During the initial stages of photoirradiation, photoreduction of GO is quite likely in addition to photocatalytic hydrogen production. However the degree to which GO is reduced by photoreduction compared to sodium borohydride is beyond the scope of this investigation. Though the photoreduction of GO is an important process for increasing the electron transfer capabilities of the composite, there are so few functional groups to be reduced compared to the amount of photocatalytic hydrogen produced, that the amount of methanol used in the photoreduction process is negligible compared to that used in the photocatalytic hydrogen production.

Figure 9i shows the photocatalytic hydrogen production graphene−$Sr_2Ta_2O_{7-x}N_x$ photocatalysts as a function of irradiation time. These materials are also compared to the $Sr_2Ta_2O_7$ and $Sr_2Ta_2O_{7-x}N_x$ photocatalysts with Pt as cocatalysts (previously shown in Figure 5i). It was clear that both the photocatalysts containing 2.5 wt % and 5 wt % graphene showed better photocatalytic hydrogen production performance than the $Sr_2Ta_2O_{7-x}N_x$-Pt without graphene, and total amounts of generated hydrogen were increased very steadily without apparent change during a testing course of over 4 h, suggesting the good stability of the composite photocatalysts. The 5 wt % graphene sample exhibited the optimized average yield of 293 μM/h (±5%) while too much graphene loading (10 wt %) was detrimental to photocatalytic hydrogen production performance. This might be attributable to the trade-off between the excellent charge transfer capability of graphene and its detrimental effect on visible light absorption. We also tested Pt-loaded graphene oxide (without photocatalyst) as a controlled sample, and the samples did not show any

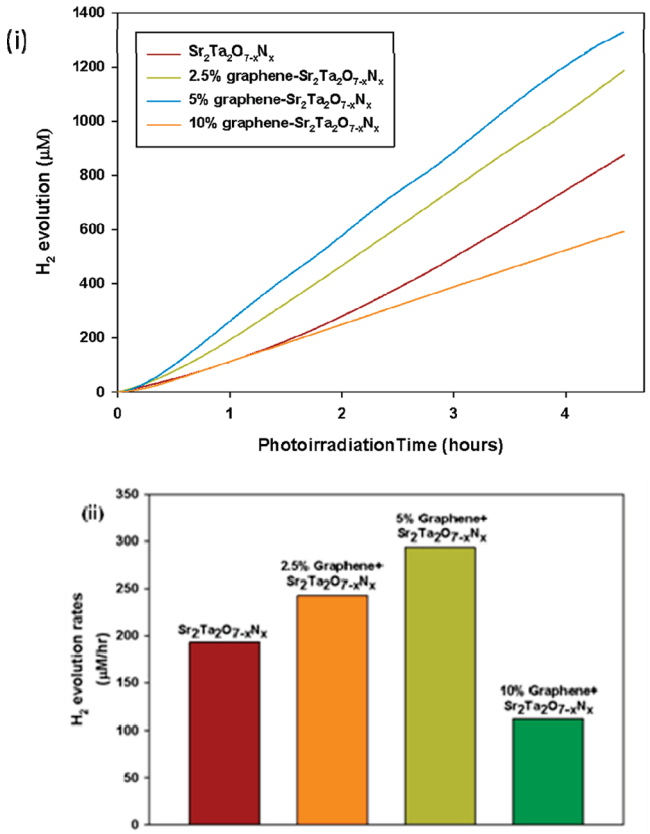

Figure 9. (i) Hydrogen evolution rates in the course of 4.5 h and (ii) hydrogen evolution rate (per hour) of various photocatalysts.

hydrogen production performance under the same experimental conditions.

It was interesting to explore the possible reason for this significant increase. As schematically demonstrated in Figure 1, charge carriers are produced when photons are irradiated onto the photocatalyst in the suspended solution. While the hole is scavenged by methanol, the electron produced is promoted to the conduction band as a result of photoexcitation. The earlier experiment with the $Sr_2Ta_2O_{7-x}N_x$ photocatalytic reduction of GO showed that electrons from the CB of the photocatalyst can be injected into the GO. Lightcap *et al.*[45] had established that, even after photoreduction, electrons can still be inserted into reduced graphene sheets. Graphene has high charge carrier mobility, and thus the electron is now mobilized on the graphene sheet. The Pt nanoclusters decorated on the graphene surface act as active sites for hydrogen evolution. The presence of graphene suspended in solution reduces the possible recombination, which in turn results in higher H_2 production in graphene composites. One issue with using graphene is that it does absorb a certain amount of light, and thus at higher graphene to $Sr_2Ta_2O_{7-x}N_x$ ratios there is a competition for light absorption. This may explain the decreasing efficiency using 10 wt % graphene.

This electron transfer scheme using a visible light photocatalyst and Pt-decorated graphene has not been reported before and is thus an innovative attempt for enhancing H_2 production yield. As mentioned earlier, the quantum efficiency for $Sr_2Ta_2O_{7-x}N_x$ with Pt cocatalyst in the wavelength of 280−550 nm was calculated to be 4.26%. This value was further improved to 6.45% (~177% increase compared to the value of 2.33% for undoped $Sr_2Ta_2O_7$) when Pt-loaded graphene scaffolds (5 wt % composite) were incorporated into the $Sr_2Ta_2O_{7-x}N_x$ photocatalyst. Thus it is clear that, through the strategic combination of nitrogen doping and using a conductive electron transport "highway", we were able to improve the hydrogen production efficiency of tantalum oxide based catalysts significantly when compared to that of the pristine $Sr_2Ta_2O_7$ photocatalyst. The efficiency is comparable to some of the well-known visible light active photocatalysts summarized in recent reports.[9,46−48] It is also worth noting that the evaluation of photocatalytic efficiency relies on the measurement of the number of molecules of hydrogen evolved as a result of photocatalysis. In general, it is still very difficult to compare the photocatalytic efficiencies in one reaction system to another, because there is still no standardized testing condition (such as the shape and size of reactors, catalyst loadings, reaction solvents, and light sources) in this field to date.[49] The quantum efficiency has thus been considered as one of the most appropriate ways of comparing photocatalyst efficiency at this stage.

In this work, we have demonstrated the feasibility of a new strategy in using graphene-functionalized nanocomposites for significant efficiency improvement in photocatalytic hydrogen production. The innovative aspects are not just the enhancement in performance but also the better understanding of crucial factors which play key roles in photocatalytic process. While the anion doping is a known technique for increasing visible light photoactivity, the findings of graphene-containing nanocomposite design is of great importance which could be applicable to other wide band gap semiconductor materials for more efficient clean energy conversion systems.

EXPERIMENTAL SECTION

Synthesis of Materials. $Sr_2Ta_2O_7$ was prepared by calcining stoichiometric mixtures of $SrCO_3$ and Ta_2O_5 powders obtained from Sigma Aldrich (purity >99%) at 1100 °C for 32 h with one intermediate grinding after 16 h by using a reported procedure.[12] Nitrogen doping of this $Sr_2Ta_2O_7$ powder was carried out by calcining these powders in ammonia atmosphere at 910 °C for 90 min, resulting in the formation of a bright yellow colored compound.

Graphite oxide (GO) was prepared through the Hummers' method,[32] by reacting commercially obtained graphite powder in a mixture of strong oxidizing agents namely H_2SO_4, $NaNO_3$, and $KMnO_4$. The GO was filtered and washed twice with 1 M HCl and twice with DI water. The GO was then dried to form a brown powder.

For photocatalytic reduction of GO experiments, light was irradiated onto the cell, using a 300 W Xe lamp (Newport, Oriel 91160) sun simulator with integrated AM1.5 filter. These reactions were carried out in an ice bath to eliminate effects of heat. A typical mixture of the ratio of (1:1 by weight) of GO (0.5 mg/mL) and $Sr_2Ta_2O_{7-x}N_x$ (0.5 mg/mL) was taken with total concentration of the mixture being 1 mg/mL in methanol. The solutions were dearated with argon for 30 min before photoirradiation as well as during the entire run. Samples were taken every 60 min and analyzed with a UV−vis spectrophotometer.

Pt nanoparticles were deposited on graphene sheets by slightly modifying an earlier known procedure.[35] GO was mixed with H_2PtCl_6 in a ratio of 10:1 in aqueous solution. A 50 mM solution of $NaBH_4$ was then added dropwise to reduce the platinum salt onto the GO scaffold. The solution turned darker as $NaBH_4$ was added due to the reduction of $[PtCl_6]^-$ to Pt metal. While the sodium borohydride reduces the platinum salt, it only partially reduces the GO. This material was then mixed with $Sr_2Ta_2O_{7-x}N_x$ in varying ratios (2.5 wt %, 5 wt %, and 10 wt % graphene−Pt).

Characterizations. X-ray diffraction (XRD) patterns of all samples were collected in the range 2°−90° (2θ) using a Bruker D8 advance X-ray diffractometer (Co Kα radiation, λ = 1.7 Å). The UV−vis absorbance spectra were obtained for the samples using a scan UV−vis spectrometer (Shimadzu UV-2450). The spectra for solid samples were obtained using an integrating sphere attachment for obtaining diffused reflectance spectra for the samples. $BaSO_4$ was used a reference. For the liquid samples absorption measurements were made using optically transparent quartz cuvettes. X-ray photoelectron spectroscopy (XPS) was carried out using a Kratos axis ULTRA X-ray photoelectron spectrometer. The binding energies were charge corrected using adventitious carbon as a reference. Elemental analysis was carried out using a flash elemental analyzer (Thermo-Flash EA1112). Real time Fourier transform infrared (FTIR) spectra were recorded using the Nicolet 6700 FT-IR. Data were recorded as percent transmittance relative to KBr, which was used as a reference.

Photocatalytic hydrogen production was carried out in an air free closed gas circulation system reaction cell made of quartz. The total cylindrical volume of the cell was 150 mL. There was an optically polished piece of quartz glass that was fused on the top of the cell to minimize light scattering. Hydrogen evolution was detected online, carried out using the setup illustrated in Supporting Information, Figure S6. Argon with a flow rate of 100 mL/min was used as a carrier gas, controlled by Brooks 5850E mass flow controller, and was passed through a quartz glass cell containing aqueous suspensions composed of 100 mg of active photocatalyst and 100 cm^3 of 20% methanol solution (electron donor) in water. The simulated sunlight was irradiated onto the reaction cell for 4.5 h using a 300 W Xe lamp (Newport, Oriel 91160) sun simulator with integrated AM1.5 filter, while the cell was cooled using a water bath to room temperature. Long-term stability tests for up to 18 h were also carried out and used to analyze the average H_2 production rate per hour. The resulting gases were continuously sampled downstream through a 25 μm capillary connected to a Varian leak valve. The leak valve introduced gases in a vacuum chamber attached to SRS RGA300 quadrupole mass spectrometer. Varian MiniTask, with a maximum pumping speed of 40 L/s (for nitrogen) and base pressure of 1.5×10^{-7} Torr, was used to evacuate the vacuum chamber. The partial pressures of the gases evolved from the sample were recorded with respect to time every 10 s. Partial pressures for H_2 were then converted to μmol/min using the calibration from a standard gas mixture (0.0994 $\pm$ 0.002% hydrogen in argon $\approx$ 53 μM/h of H_2) at the same flow rate of 100 mL/min. The whole system, including the photocatalyst, was flushed with Ar at 100 mL/min for 1 h to remove any trace of air (including nitrogen and oxygen) before every photocatalytic reaction was carried out.

Acknowledgment. This project was supported by Australian Research Council (through its Centres of Excellence grant and DP programs) and Queensland State Government (NIRAP).

Supporting Information Available: Additional TEM images, XRD patterns, FTIR spectra, UV−visible spectra, quantum efficiency calculations, and the photocatalyst evaluation schematic used. This material is available free of charge *via* the Internet at http://pubs.acs.org.

REFERENCES AND NOTES

1. Bockris, J. O. The Origin of Ideas on a Hydrogen Economy and Its Solution to the Decay of the Environment. *Int. J. Hydrogen Energy* **2002,** *27*, 731–740.
2. Navarro Yerga, R. M.; Álvarez Galván, M. C.; del Valle, F.; Villoria de la Mano, J. A.; Fierro, J. L. G. Water Splitting on Semiconductor Catalysts under Visible-Light Irradiation. *ChemSusChem* **2009,** *2*, 471–485.
3. Ravelli, D.; Dondi, D.; Fagnoni, M.; Albini, A. Photocatalysis. A Multifaceted Concept for Green Chemistry. *Chem. Soc. Rev.* **2009,** *38*, 1999–2011.
4. Turner, J. A. A Realizable Renewable Energy Future. *Science* **1999,** *285*, 687–689.
5. Fujishima, A.; Honda, K. Electrochemical Photolysis of Water at a Semiconductor Electrode. *Nature* **1972,** *238*, 37–38.
6. Tryk, D. A.; Fujishima, A.; Honda, K. Recent Topics in Photoelectrochemistry: Achievements and Future Prospects. *Electrochim. Acta* **2000,** *45*, 2363–2376.
7. Osterloh, F. E. Inorganic Materials as Catalysts for Photochemical Splitting of Water. *Chem. Mater.* **2007,** *20*, 35–54.
8. Kitano, M.; Hara, M. Heterogeneous Photocatalytic Cleavage of Water. *J. Mater. Chem.* **2010,** *20*, 627–641.
9. Kudo, A.; Miseki, Y. Heterogeneous Photocatalyst Materials for Water Splitting. *Chem. Soc. Rev.* **2009,** *38*, 253–278.
10. Kudo, A. Photocatalysis and Solar Hydrogen Production. *Pure Appl. Chem.* **2007,** *79*, 1917–1927.

11. Kudo, A.; Kato, H.; Nakagawa, S. Water Splitting into H_2 and O_2 on New $Sr_2M_2O_7$ (M = Nb and Ta) Photocatalysts with Layered Perovskite Structures: Factors Affecting the Photocatalytic Activity. *J. Phys. Chem. B* **1999,** *104*, 571–575.
12. Asahi, R.; Morikawa, T.; Ohwaki, T.; Aoki, K.; Taga, Y. Visible-Light Photocatalysis in Nitrogen-Doped Titanium Oxides. *Science* **2001,** *293*, 269–271.
13. Burda, C.; Lou, Y.; Chen, X.; Samia, A. C. S.; Stout, J.; Gole, J. L. Enhanced Nitrogen Doping in TiO_2 Nanoparticles. *Nano Lett.* **2003,** *3*, 1049–1051.
14. Ohno, T.; Akiyoshi, M.; Umebayashi, T.; Asai, K.; Mitsui, T.; Matsumura, M. Preparation of S-doped TiO_2 Photocatalysts and Their Photocatalytic Activities under Visible Light. *Appl. Catal. A* **2004,** *265*, 115–121.
15. Umebayashi, T.; Yamaki, T.; Itoh, H.; Asai, K. Band Gap Narrowing of Titanium Dioxide by Sulfur Doping. *Appl. Phys. Lett.* **2002,** 454.
16. Khan, S. U. M.; Al-Shahry, M.; Ingler, W. B. Efficient Photochemical Water Splitting by a Chemically Modified *n*-TiO_2. *Science* **2002,** *297*, 2243–2245.
17. Abe, R.; Higashi, M.; Domen, K. Facile Fabrication of an Efficient Oxynitride TaON Photoanode for Overall Water Splitting into H_2 and O_2 under Visible Light Irradiation. *J. Am. Chem. Soc.* **2010,** *132*, 11828–11829.
18. Maeda, K.; Domen, K. Photocatalytic Water Splitting: Recent Progress and Future Challenges. *J. Phys. Chem. Lett.* **2010,** *1*, 2655–2661.
19. Maeda, K.; Domen, K. New Nonoxide Photocatalysts Designed for Overall Water Splitting under Visible Light. *J. Phys. Chem. C* **2007,** *111*, 7851–7861.
20. Liu, G.; Wang, L. Z.; Sun, C.; Yan, X.; Wang, X.; Chen, Z.; Smith, S. C.; Cheng, H. M.; Lu, G. Q. Band-to-Band Visible-Light Photon Excitation and Photoactivity Induced by Homogeneous Nitrogen Doping in Layered Titanates. *Chem. Mater.* **2009,** *21*, 1266–1274.
21. Mukherji, A.; Marschall, R.; Tanksale, A.; Sun, C.; Smith, S. C.; Lu, G. Q.; Wang, L. Z. N-Doped $CsTaWO_6$ as a New Photocatalyst for Hydrogen Production from Water Splitting Under Solar Irradiation. *Adv. Funct. Mater.* **2011,** *21*, 126–132.
22. Skinner, D. E.; Colombo, D. P.; Cavaleri, J. J.; Bowman, R. M. Femtosecond Investigation of Electron Trapping in Semiconductor Nanoclusters. *J. Phys. Chem.* **1995,** *99*, 7853–7856.
23. Philip Colombo, D.; Roussel, K. A.; Saeh, J.; Skinner, D. E.; Cavaleri, J. J.; Bowman, R. M. Femtosecond Study of the Intensity Dependence of Electron-Hole Dynamics in TiO_2 Nanoclusters. *Chem. Phys. Lett.* **1995,** *232*, 207–214.
24. Tada, H.; Kiyonaga, T.; Naya, S. I. Rational Design and Applications of Highly Efficient Reaction Systems Photocatalyzed by Noble Metal Nanoparticle-Loaded Titanium(IV) Dioxide. *Chem. Soc. Rev.* **2009,** *38*, 1849–1858.
25. Costamagna, P.; Srinivasan, S. Quantum Jumps in the PEMFC Science and Technology from the 1960s to the Year 2000: Part II. Engineering, Technology Development and Application Aspects. *J. Power Sources* **2001,** *102*, 253–269.
26. Kongkanand, A.; Martínez Domínguez, R.; Kamat, P. V. Single Wall Carbon Nanotube Scaffolds for Photoelectrochemical Solar Cells. Capture and Transport of Photogenerated Electrons. *Nano Lett.* **2007,** 676–680.
27. Ng, Y. H.; Lightcap, I. V.; Goodwin, K.; Matsumura, M.; Kamat, P. V. To What Extent Do Graphene Scaffolds Improve the Photovoltaic and Photocatalytic Response of TiO_2 Nanostructured Films? *J Phys. Chem. Lett.* **2010,** *1*, 2222–2227.
28. Geim, A. K.; Novoselov, K. S. The Rise of Graphene. *Nat. Mater.* **2007,** *6*, 183–191.
29. Stankovich, S.; Dikin, D. A.; Dommett, G. H. B.; Kohlhaas, K. M. E. J.; Zimney; Stach, E. A.; Piner, R. D.; Nguyen, S. T.; Ruoff, R. S. Graphene-Based Composite Materials. *Nature* **2006,** *442*, 282–286.
30. Nair, R. R.; Blake, P.; Grigorenko, A. N.; Novoselov, K. S.; Booth, T. J.; Stauber, T.; Peres, N. M. R.; Geim, A. K. Fine Structure Constant Defines Visual Transparency of Graphene. *Science* **2008,** *320*, 1308.
31. McAllister, M. J.; Li, J. L.; Adamson, D. H.; Schniepp, H. C.; Abdala, A. A.; Liu, J.; Herrera-Alonso, M.; Milius, D. L.; Car, R.; Prud'homme, R. K.; Aksay, I. A. Single Sheet Functionalized Graphene by Oxidation and Thermal Expansion of Graphite. *Chem. Mater.* **2007,** *19*, 4396–4404.
32. Hummers, W. S.; Offeman, R. E. Preparation of Graphitic Oxide. *J. Am. Chem. Soc.* **1958,** *80*, 1339.
33. Staudenmaier, L. Preparation of Graphitic Acid. *Ber. Dtsch. Chem. Ges.* **1898,** *31*, 1481.
34. Li, D.; Muller, M. B.; Gilje, S.; Kaner, R. B.; Wallace, G. G. Processable Aqueous Dispersions of Graphene Nanosheets. *Nat. Nanotechnol.* **2008,** *3*, 101–105.
35. Williams, G.; Seger, B.; Kamat, P. V. TiO_2-Graphene Nanocomposites. UV-Assisted Photocatalytic Reduction of Graphene Oxide. *ACS Nano* **2008,** *2*, 1487–1491.
36. Williams, G.; Kamat, P. V. Graphene-Semiconductor Nanocomposites: Excited-State Interactions between ZnO Nanoparticles and Graphene Oxide. *Langmuir* **2009,** *25*, 13869–13873.
37. Yang, N.; Zhai, J.; Wang, D.; Chen, Y.; Jiang, L Two-Dimensional Graphene Bridges Enhanced Photoinduced Charge Transport in Dye-Sensitized Solar Cells. *ACS Nano* **2010,** *4*, 887–894.
38. Seger, B.; Kamat, P. V. Electrocatalytically Active Graphene-Platinum Nanocomposites. Role of 2-D Carbon Support in PEM Fuel Cells. *J. Phys. Chem. C* **2009,** *13*, 7990–7995.
39. Yoo, E.; Okata, T.; Akita, T.; Kohyama, M.; Nakamura, J.; Honma, I. Enhanced Electrocatalytic Activity of Pt Subnanoclusters on Graphene Nanosheet Surface. *Nano Lett.* **2009,** *9*, 2255–2259.
40. Ng, Y. H.; Iwase, A.; Kudo, A.; Amal, R. Reducing Graphene Oxide on a Visible-Light $BiVO_4$ Photocatalyst for an Enhanced Photoelectrochemical Water Splitting. *J. Phys. Chem. Lett.* **2010,** *1*, 2607–2612.
41. Ji, M. S.; Borse, P. H.; Kim, H. G.; Hwang, D. W.; Jang, J. K.; Bae, S. W.; L., J. S. Photocatalytic Hydrogen Production from Water−Methanol Mixtures Using N-Doped $Sr_2Nb_2O_7$ under Visible Light Irradiation: Effects of Catalyst Structure. *Phys. Chem. Chem. Phys.* **2005,** *7*, 1315–1321.
42. Hara, M.; Chiba, E.; Ishikawa, A.; Takata, T.; Kondo, J. N.; Domen, K. Ta_3N_5 and TaON Thin Films on Ta Foil: Surface Composition and Stability. *J. Phys. Chem. B.* **2003,** *107*, 13441–13445.
43. Kongkanand, A.; Kamat, P. V. Electron Storage in Single Wall Carbon Nanotubes. Fermi Level Equilibration in Semiconductor−SWCNT Suspensions. *ACS Nano* **2007,** *1*, 13–21.
44. Becerril, H. A.; Mao, J.; Liu, Z.; Stoltenberg, R. M.; Bao, Z.; Chen, Y. Evaluation of Solution-Processed Reduced Graphene Oxide Films as Transparent Conductors. *ACS Nano* **2008,** *2*, 463–470.
45. Lightcap, I. V.; Kosel, T. H.; Kamat, P. V. Anchoring Semiconductor and Metal Nanoparticles on a Two-Dimensional Catalyst Mat. Storing and Shuttling Electrons with Reduced Graphene Oxide. *Nano Lett.* **2010,** *10*, 577–583.
46. Miseki, Y.; Kudo, A. Water Splitting over New Niobate Photocatalysts with Tungsten−Bronze-Type Structure and Effect of Transition Metal-Doping. *ChemSusChem.* **2011,** *4*, 245–251.
47. Chen, X. B.; Shen, S. H.; Guo, L. J.; Mao, S. S. Semiconductor-Based Photocatalytic Hydrogen Generation. *Chem. Rev.* **2010,** *110*, 6503–6570.
48. Hu, C. C.; Lee, Y. L.; Teng, H. Efficient Water Splitting over $Na_{1-x}K_xTaO_3$ Photocatalysts with Cubic Perovskite Structure. *J. Mater. Chem.* **2011,** *21*, 3824–3830.
49. Maschmeyer, T.; Che, M Catalytic Aspects of Light-Induced Hydrogen Generation in Water with TiO_2 and Other Photocatalysts: A Simple and Practical Way towards a Normalization? *Angew Chem., Int. Ed.* **2010,** *49*, 1536–1539.